

# pp Elastic Scattering at LHC and Nucleon Structure

M. M. Islam<sup>a;1</sup>, R. J. Luddy<sup>a;2</sup> and A. V. Prokudin<sup>b;c;3</sup>

(a) Department of Physics, University of Connecticut, Storrs, CT 06269, USA  
 (b) Dipartimento di Fisica Teorica, Università degli Studi di Torino, Via Pietro Giuria 1, 10125 Torino, ITALY and Sezione INFN di Torino, ITALY  
 (c) Institute For High Energy Physics, 142281 Protvino, RUSSIA

## Abstract

High energy elastic pp scattering at the Large Hadron Collider (LHC) at cm. energy 14 TeV is predicted using the asymptotic behavior of  $\sigma_{\text{tot}}(s)$  and  $\sigma(s)$  known from dispersion relation calculations and the measured elastic pp differential cross section at  $\sqrt{s} = 546$  GeV. The effective field theory model underlying the phenomenological analysis describes the nucleon as having an outer cloud of quark-antiquark condensed ground state, an inner core of topological baryonic charge of radius  $0.44$  fm and a still smaller valence quark-bag of radius  $0.1$  fm. The LHC experiment TOTEM (Total and Elastic Measurement), if carried out with sufficient precision from  $|j| = 0$  to  $|j| > 10$  GeV $^2$ , will be able to test this structure of the nucleon.

High-energy elastic pp and  $\bar{p}p$  scattering have been measured at CERN ISR [1] and SPS Collider [2] and at Fermilab [3], [4] over the energy range  $\sqrt{s} = 23.5$  GeV to 1.8 TeV. These measurements provide a broad perspective of the energy dependence of elastic differential cross sections and of the asymptotic behavior of total cross section  $\sigma_{\text{tot}}(s)$  and of the ratio of real to imaginary part of the forward amplitude  $\sigma(s)$ . They have led to various phenomenological models of elastic scattering, such as (1) impact-picture model [5], (2) Regge pole-cut models [6], [7], (3) QCD motivated eikonal model [8], (4) cloud-core model [9]. Theoretical investigation of the last model has shown that an effective field theory model with quarks interacting via a scalar field underlies it [10]. Soft diffraction processes mediated by pions including high-mass diffraction dissociation have also been proposed to describe elastic scattering at LHC for small  $|j| < 0.5$  GeV $^2$  [11].

Study of the field theory model further indicates that the nucleon has an outer cloud of quark-antiquark condensed ground state analogous to a superconducting state, an inner core of topological baryonic charge and a still smaller quark-bag of valence quarks. The elastic scattering experiment TOTEM at LHC [12], if carried out with sufficient precision, will be able to identify these three regions inside the nucleon by their characteristic behaviors reflected in the elastic differential cross section. The present investigation reports our quantitative prediction of differential cross section at LHC at  $\sqrt{s} = 14$  TeV.

<sup>1</sup>E-mail: islam@phys.uconn.edu

<sup>2</sup>E-mail: rjuddy@attbi.com

<sup>3</sup>E-mail: prokudin@to.infn.it

Preliminary calculation of this differential cross section was reported earlier [13]. We show how the behavior of  $d\sigma/dt$  in different ranges of  $|t|$  relates with the three regions inside the nucleon. The parameters in our model are determined such that the high-energy asymptotic behavior of  $\sigma_{tot}(s)$  and  $\sigma_{D^+}(s)$  based on dispersion relation [4] and the measured elastic pp differential cross section at  $\sqrt{s} = 546$  GeV [2] are satisfactorily described. General asymptotic requirements of the interaction amplitude are shown to be satisfied by our phenomenological interaction amplitude. We also present our predicted pp elastic differential cross section at  $\sqrt{s} = 500$  GeV (measurement of which is planned at the Relativistic Heavy Ion Collider [15]).

We describe the crossing even (C-even) interaction amplitude using the impact parameter representation

$$T_D^+(s; t) = \frac{1}{ipW} \int_0^{Z_1} b db J_0(bq) \sigma_D^+(s; b) \quad (1)$$

with a profile function [9]

$$\sigma_D^+(s; b) = g(s) \frac{h}{1 + \exp[(b - R)/a]} + \frac{1}{1 + \exp[-(b + R)/a]} \quad (2)$$

where  $W = \frac{p}{s}$ ,  $q = \frac{p}{t}$ ,  $R$  and  $a$  are energy dependent  $R(s) = R_0 + R_1(\ln s - 2)$ ,  $a(s) = a_0 + a_1(\ln s - 2)$ .  $g(s)$  is a crossing even function:  $g(se^i) = g(s)$  which asymptotically goes to a real positive constant. Besides the interaction amplitude, the model has a hard scattering amplitude originating from one nucleon core scattering on the other core via vector meson exchange, while their outer clouds overlap and interact independently. The hard scattering amplitude is given by an amplitude  $T_1(s; t)$  due to a single hard collision multiplied by an absorption factor  $[1 - \frac{pp}{D}(s; 0)]$  or  $[1 - \frac{pp}{D}(s; 0)]$ . In the absorption factor, the possibility of a C-odd contribution at zero impact parameter is taken into account, so that  $\frac{pp}{D}(s; 0) = \frac{+}{D}(s; 0) + \frac{-}{D}(s; 0)$ ,  $\frac{pp}{D}(s; 0) = \frac{+}{D}(s; 0) - \frac{-}{D}(s; 0)$ .

The interaction amplitude obtained from Eqs.(1) and (2) satisfies the general properties associated with the phenomenology of interaction:

1. It leads to  $\sigma_{tot}(s) \sim (a_0 + a_1 \ln s)^2$ , i.e. qualitative saturation of Froissart-Martin bound.
2. It yields  $\sigma(s) \sim a_0 + a_1 \ln s$  asymptotically, so that the derivative dispersion relation result [16]  $\sigma'(s) = \sigma''(s) = \ln s$  is satisfied.
3. It obeys the Auberson-Kinoshita-Martin scaling, i.e.  $T_D^+(s; t) \sim \ln^2(s) / (|t| \ln^2 s)$  asymptotically.
4. It is C-even, and therefore yields equal pp and pp total and differential cross sections.

The asymptotic properties 1–3 of the di reaction amplitude  $T_D^+(s; t)$  can be seen in the following way: We express the profile function  $\frac{1}{D}(s; b)$  in the form

$$\frac{1}{D}(s; b) = g(s) \frac{\sinh R = a}{\cosh R = a + \cosh b = a} : \quad (3)$$

Then we change the variable of integration from  $b$  to  $b = a$  and rotate the line of integration a little to the real axis. This leads to

$$T_D^+(s; t) = i p W g(s) a^2 \int_0^{\infty} d q \frac{\sinh R = a}{\cosh R = a + \cosh q = a} : \quad (4)$$

We observe that, when  $a_0 + a_1 \ln s \gg 1$ ,

$$\frac{R_0 + R_1 (\ln s - i = 2)}{a_0 + a_1 (\ln s - i = 2)} = \frac{R_0 - ra}{a_0 + a_1 (\ln s - i = 2)} + r' - r; \quad (5)$$

where  $r = R_1/a_1$  is a real quantity. Using this in the integrand in (4), we obtain the first three properties. The fourth one follows from the C-even form (2) of the profile function. We note that the  $\ln s$  dependence in the di reaction amplitude always occurs in the combination  $(a_0 + a_1 \ln s)$ , which is independent of the scale of  $s$ .

For  $|t| \neq 0$ ,  $T_D^+(s; t)$  is given by the crossing symmetric form [9]

$$T_D^+(s; t) = i g(s) a \frac{1}{2} f - i(R + i a) H_0^{(1)}[q(R + i a)] + i(R - i a) H_0^{(2)}[q(R - i a)] g : \quad (6)$$

When  $qR - i a \gg 1$ , the Hankel functions fall off exponentially, which leads to  $|T_D^+(s; t)| \approx \exp[-q(a + a_1 \ln s)]$  as  $s \gg 1$ . Since  $d = dt = 4 \pi (s; t) = s^2$ , we find that for  $q$  fixed and  $s \gg 1$ , the differential cross section due to di reaction vanishes. On the other hand, the total cross section due to di reaction tends to infinity as  $\ln^2 s$ . Hence, Martin's theorem [17] predicts a zero of  $\text{Re } T_D^+(s; t)$  in the near forward direction. Indeed, in our calculations we find such zeros indicating further the asymptotic nature of our di reaction amplitude.

To extend our previous calculations to the LHC energy, we needed a way to determine the  $s$  dependence of  $g(s)$ . Accurate model independent analysis by K undrat and Loka jíøek [18] has shown that inelasticity due to di reaction at  $b = 0$ , i.e.  $\exp[i \frac{1}{D}(s; 0)]$  is small but finite at high energy and decreases slowly with increasing  $s$ . This has led us to consider the following simple crossing even parametrization:

$$e^{i \frac{1}{D}(s; 0)} = g_0 + \frac{C_0}{(s e^{i \pi/2})} : \quad (7)$$

As  $g(s)$  is related to  $\exp[i \frac{1}{D}(s; 0)] = 1 + \frac{1}{D}(s; 0)$  via Eq.(3), the three energy independent parameters in (7) together with other di reaction parameters allow us to obtain  $g(s)$  at different values of  $s$ . To take into account the energy dependence of  $\frac{1}{D}(s; 0)$ , we have assumed a similar parametrization:

$$\frac{1}{D}(s; 0) = i g_0 - \frac{i \frac{d_0}{(s e^{i \pi/2})}}{(s e^{i \pi/2})} ; \quad (8)$$

which of course has the required crossing odd property. Finally, for the energy dependence of the term  $\hat{^0}(s)\exp[i\hat{^0}(s)] = \sim \exp[i\hat{^0}(s;0)]$ , we have taken the parametrization:

$$\hat{^0}(s)\exp[i\hat{^0}(s)] = \hat{^0}_0 + \frac{\hat{^1}_1}{(\sin^{\frac{1}{2}})^{\hat{^0}}}: \quad (9)$$

We note an odderon contribution (an asymptotic crossing-odd amplitude) in our analysis:

$$s\hat{^0}_0 \frac{F^2(t)}{m^2} \frac{1}{t} (+ \text{ sign for } pp; - \text{ sign for } \bar{pp}); \quad (10)$$

where  $F(t)$  is the  $^1\text{NN}$  form factor. As in the previous work [9], we take

$$F^2(t) = (m^2 - t)^{1/2} K_1[(m^2 - t)^{1/2}]: \quad (11)$$

This corresponds to a smoothed Yukawa potential  $e^{-m(r^2 + t^2)^{1/2}} = (r^2 + t^2)^{1/2}$  between nucleons due to  $\pi$  exchange and leads to an exponential fall-off (or rear fall-off) of the differential cross section:  $d\sigma/dt = \exp(-2\pi^2 t^2)$ , when hard scattering dominates.

There are now thirteen energy-independent parameters in our model:  $R_0, R_1, a_0, a_1, \alpha_0, \alpha_1, \beta_0, \beta_1, d_0, \hat{^0}_0, \hat{^1}_1, \hat{^0}, \hat{^1}$ . As mentioned earlier, we determine these parameters by requiring that they satisfactorily describe the high energy asymptotic behavior of  $\sigma_{\text{tot}}(s)$  and  $\sigma_{\text{pp}}(s)$  given by dispersion relation calculations [4] and the experimental  $^1\text{p-}$  elastic differential cross section at  $\sqrt{s} = 546 \text{ GeV}$  [2]. The values of the parameters obtained by us are:  $R_0 = 2.50, R_1 = 0.0385, a_0 = 0.57, a_1 = 0.106, \alpha_0 = 0.02, \alpha_1 = 1.40, \beta_0 = 0.50, \beta_1 = 0.375, d_0 = 13.0, \hat{^0}_0 = 0.38, \hat{^1}_1 = 2.81, \hat{^0}_1 = 400.0, \hat{^1}_0 = 1.30$ . (Our unit of energy is 1 GeV.)  $\hat{^0}_0$  and  $\hat{^1}_1$  are not free parameters in our present analysis. They are kept fixed at values found previously:  $\hat{^0}_0 = 3.075, \hat{^1}_1 = 0.801$ , which correspond to a radius 0.44 fm for the nucleon repulsive core.

In Fig.1, our calculated  $\sigma_{\text{tot}}(s)$  is shown as a function of  $\sqrt{s}$  (solid curve). We find  $\sigma_{\text{tot}}(s)$  for  $pp$  and  $\bar{pp}$  essentially overlap. The dotted lines represent the region of uncertainty for  $\sigma_{\text{tot}}(s)$  obtained by Augier et al. [4] from dispersion relation calculations [19]. In Fig.2, we show our calculated  $\sigma_{\text{pp}}(s)$  as a function of  $\sqrt{s}$  (solid curve:  $pp$ , dashed curve:  $\bar{pp}$ ). As in Fig.1, the dotted lines represent the region of uncertainty for  $\sigma_{\text{pp}}(s)$  obtained by Augier et al. [4]. Experimental data are shown for comparison with the theoretical calculations. In Fig.3, we show our calculated  $d\sigma/dt$  for  $pp$  at  $\sqrt{s} = 546 \text{ GeV}$  (solid curve) together with the experimental data of Bozzo et al. [2]. Also shown are  $d\sigma/dt$  due to diffraction alone (dotted curve) and due to hard scattering alone (dot-dashed curve). As in earlier calculations, there is destructive interference between diffraction amplitude and the hard scattering amplitude resulting in a dip at  $t = 1.0 \text{ GeV}^2$ . The thick-dashed curve in Fig.3 shows our predicted  $d\sigma/dt$  for  $pp$  elastic scattering at  $\sqrt{s} = 500 \text{ GeV}$ , which will be measured at RHIC in the small  $|t|$  region [15].

With the parameters determined from  $\sigma_{\text{tot}}(s)$  (Fig.1),  $\sigma_{\text{pp}}(s)$  (Fig.2), and  $d\sigma/dt$  at 546 GeV (Fig.3), we have asked ourselves: What are our predictions for  $d\sigma/dt$  at  $\sqrt{s} = 1.8 \text{ TeV}$  and  $\sqrt{s} = 630 \text{ GeV}$ , and how do they compare with the existing experimental

measurements? The results are shown in Figs.4 and 5. As can be seen, our description of the differential cross section at 1.8 TeV is quite satisfactory. As for the differential cross section at 630 GeV, we notice that the predicted  $d/dt$  for  $|t| > 1 \text{ GeV}^2$  is higher than the large  $|t|$  data [21]. This reflects the fact that non-asympotic terms are present in our analysis and contribute non-negligibly to  $d/dt$  for large  $|t|$ . This is also seen in Fig.3 for pp differential cross section at 546 GeV. Our model describes the asymptotic behavior and the approach to the asymptotic behavior of the elastic scattering amplitude. But, it cannot exclude the possibility of non-asympotic terms contributing at some finite high energy such as 630 GeV and 546 GeV. The fact that our hard scattering contribution alone accounts for the large  $|t|$  differential cross section at 630 GeV and 546 GeV supports the point that the core-core scattering is showing up. Furthermore, it is because of the possibility of non-asympotic terms being present that we determine our parameters not by  $\chi^2$  analysis, but by requiring that they describe well  $\sigma_{\text{tot}}(s)$ ,  $\sigma(s)$  and  $d/dt$  at 546 GeV. Finally, as far as odderon contribution to  $d/dt$  is concerned, we find it quite small and only noticeable in the dip region.

In Fig.6, we show our predicted pp elastic differential cross section at the LHC cm. energy 14 TeV (solid curve). Also shown for comparison are  $d/dt$  predicted by the impact picture model at  $\sqrt{s} = 14 \text{ TeV}$  (dashed curve) and  $d/dt$  predicted by the Regge pole-cut model at  $\sqrt{s} = 16 \text{ TeV}$  (dot-dashed curve) [5], [6], [20]. We find that the real part of the differential cross section has a zero at  $|t| = 0.087 \text{ GeV}^2$  as expected from Martin's theorem [17]. The dotted line in Fig.6 represents schematically the expected change in our model in the behavior of  $d/dt$  from 0 near  $|t| = 0$  :  $d/dt \propto e^{\alpha|t|}$  to a power fall-off :  $d/dt \propto 1/t^0$  due to quark-quark scattering [10], [22]. It corresponds to a transition from the nonperturbative regime to the perturbative regime and should appear as a distinct change in the slope of  $d/dt$  at large  $|t| > 8 \text{ GeV}^2$  [23]. We further note that in our model  $d/dt$  falls off smoothly for  $|t| < 1.5 \text{ GeV}^2$ . On the other hand, impact-picture model and Regge pole-cut model predict in this  $|t|$  region oscillatory behavior typical of diffraction models [20].

In conclusion, we have been able to extend previous pp, pp elastic  $d/dt$  calculations at ISR and SPS Collider energies [9] to the high energy asymptotic region. This has been possible by parameterizing the energy-dependent parameters suitably consistent with their crossing properties and by requiring that the model describes satisfactorily: (1) the high energy behavior of  $\sigma_{\text{tot}}(s)$  and  $\sigma(s)$  as given by dispersion relation calculations, and (2) the experimentally measured elastic pp differential cross section at  $\sqrt{s} = 546 \text{ GeV}$ . We then obtain a quantitative prediction of pp elastic  $d/dt$  at LHC at the cm. energy 14 TeV. Our phenomenological investigation of elastic pp and pp scattering is based on nucleon having an outer cloud of quark-antiquark condensed state, an inner core of topological baryonic charge, and a much smaller quark-bag of radius  $\sim 0.1 \text{ fm}$  [10]. Correspondingly, in  $d/dt$  we have diffraction scattering dominating the small  $|t|$  region, hard scattering dominating the intermediate  $|t|$  region ( $1.5 < |t| < 8.0 \text{ GeV}^2$ ) and quark-quark scattering taking over in the large  $|t|$  region (see Fig.6). The  $|t|$  dependence of these three regions are very different, so that accurate measurement of  $d/dt$  in the TOTEM experiment [12] will be able to identify

these three regions. We also note that the underlying field theory model of the above nucleon structure based on gauged linear model indicates that the transition from the nonperturbative regime of diffraction and hard scattering to the perturbative regime of quark-quark scattering is a chiral phase transition [10]. Therefore, observation of a distinct change in the slope of  $d = dt$  at large  $|t| > 8.0 \text{ GeV}^2$  will provide an important signature of this phase transition.

The authors would like to thank Enrico Predazzi for his interest and comments. R JL would like to thank Ben Luddy for his programming assistance. M MI would like to thank Mike Abbott for bringing Fermilab E-811 Collaboration result to his attention.

## R eferences

- [1] E Nagy et al., Nucl. Phys. B 150 (1979) 221.
- [2] UA4 Collaboration, M Bozzo et al., Phys. Lett. B 147 (1984) 385; Phys. Lett. B 155 (1985) 197.
- [3] N Amos et al., Phys. Lett. B 247 (1990) 127.
- [4] F Abe et al., Phys. Rev. D 50 (1994) 5518.
- [5] C Bourrely, J. Soffer, and T.T. Wu, Phys. Rev. Lett. 54 (1985) 757; in *Frontiers in Strong Interactions*, ed by P. Chiappetta, M. Aguenauer, and J. Tran Thanh Van (Editions Frontières, 1996) p.15.
- [6] P Desgrolard, M. Giron, and E. Predazzi, Z. Phys. C 63 (1994) 241.
- [7] V.A. Petrov and A.V. Prokudin, Eur. Phys. J. C 23 (2002) 135.
- [8] M.M. Block, E.M. Gregores, F. Halzen, and G. Pancheri, Phys. Rev. D 60 (1999) 054024.
- [9] M.M. Islam, V. Innocente, T. Fearnley, and G. Sanguinetti, Europhys. Lett. 4 (1987) 189.
- [10] M.M. Islam, in Proc. of the Fifth Workshop on Quantum Chromodynamics, ed by H.M. Fried, B.M. Uller, and Y. Gabellini (World Scientific, 2000) p.269.
- [11] V.A. Khoze, A.D. Martin, and M.G. Ryskin, Eur. Phys. J. C 18 (2000) 167.
- [12] G. Matthiae, in Proc. of the IXth Blois Workshop on Elastic and Diffractive Scattering, ed. by V. Kunderat and P. Zavada (Institute of Physics AS CR, Prague, 2002) p.355.
- [13] M.M. Islam and E.M. Kubik, in Proc. of the VIIIth Blois Workshop on Elastic and Diffractive Scattering, ed. by V.A. Petrov and A.V. Prokudin (World Scientific, 2000) p.325.

[14] C Augier et al., *Phys. Lett. B* 315 (1993) 503.

[15] W Guryan, *Nucl. Phys. (Proc. Suppl.) B* 99 (2001) 299.  
Kushik De, in *Proc. of the IXth Blois Workshop*, *ibid.*, p.63.

[16] M M Block, K Kang, and A R White, *Int. Jour. of Mod. Phys. A* 7 (1992) 4449.

[17] A Martin, *Phys. Lett. B* 404 (1997) 137.

[18] V Kudrat and M Lokaříček, *Z. Phys. C* 63 (1994) 619.

[19] Recent analysis by Fermilab E-811 Collaboration (Avila et al., *Phys. Lett. B* 537 (2002) 41) corroborates previous calculations of Augier et al. [14].

[20] M Buenerd, in *Frontiers in Strong Interactions*, *ibid.* p. 437.

[21] D. Bernard et al., *Phys. Lett. B* 171 (1986) 142.

[22] M G Sotiropoulos and G Sternan, *Nucl. Phys. B* 425 (1994) 489.

[23] This estimate of  $\langle jj \rangle$  is based on our earlier investigation of  $d\langle dt \rangle$  at  $\sqrt{s} = 53 \text{ GeV}$ . ISR data indicate a change in slope for  $\langle jj \rangle > 6.0 \text{ GeV}^2$  (H De Kerret et al., *Phys. Lett. B* 68 (1977) 374).

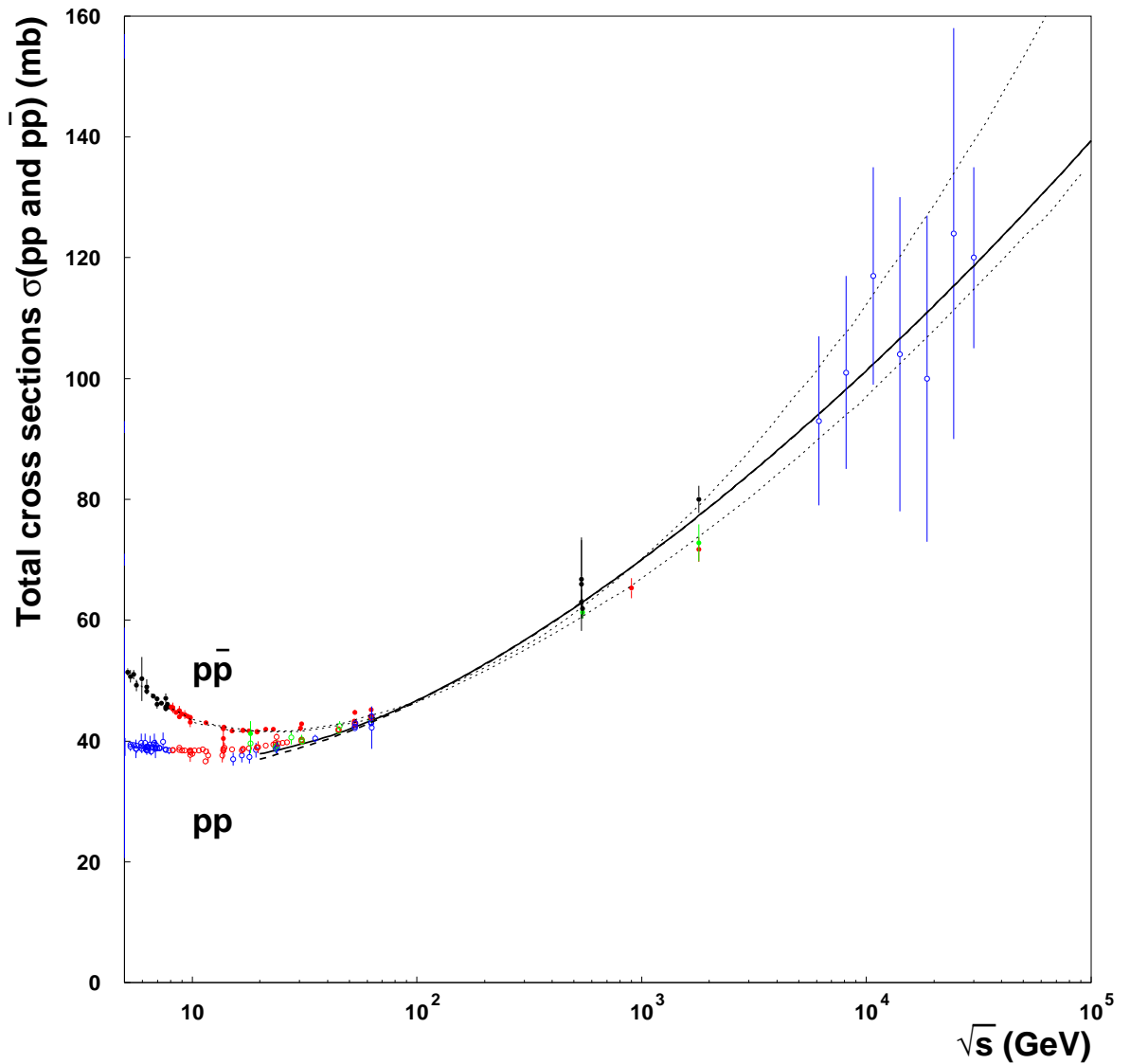


Figure 1: Our calculated  $\sigma_{pp}^{\text{tot}}$  (solid line) and  $\sigma_{p\bar{p}}^{\text{tot}}$  (dashed line) are shown as functions of  $\sqrt{s}$ . Total cross sections for  $pp$  and  $p\bar{p}$  essentially overlap. The dotted lines represent the region of uncertainty for  $\sigma_{pp}^{\text{tot}}$  obtained from dispersion relation calculations [14]. Experimental data are given for comparison.

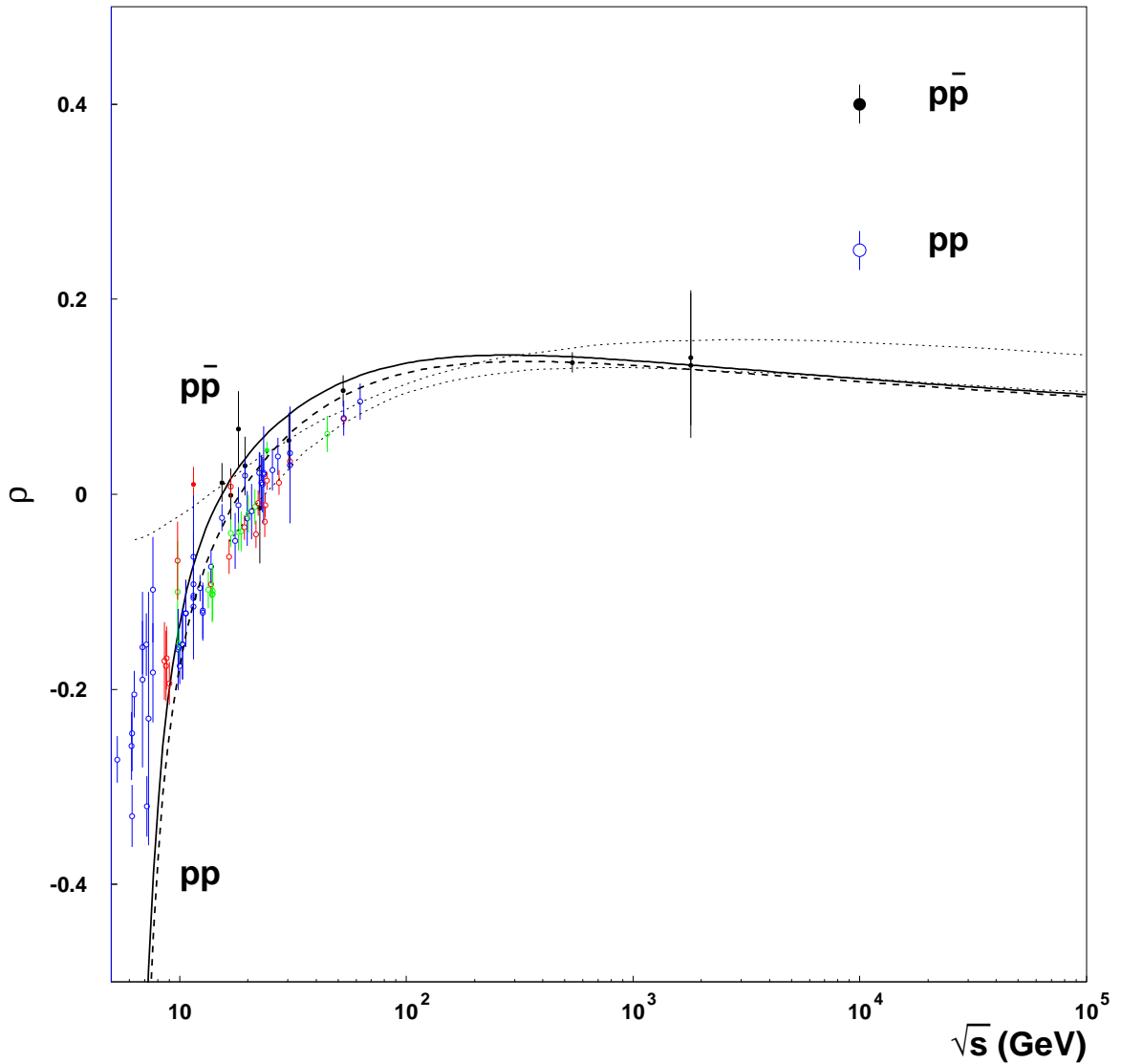


Figure 2:  $P(s) = \text{Re}T(s; 0) = \text{Im}T(s; 0)$  calculated by us is shown as a function of  $\sqrt{s}$ . Solid curve corresponds to  $p\bar{p}$  and dashed curve to  $p p$ . The dotted lines represent the region of uncertainty for  $P(s)$  obtained from dispersion relation calculations [4]. Experimental data are given for comparison.

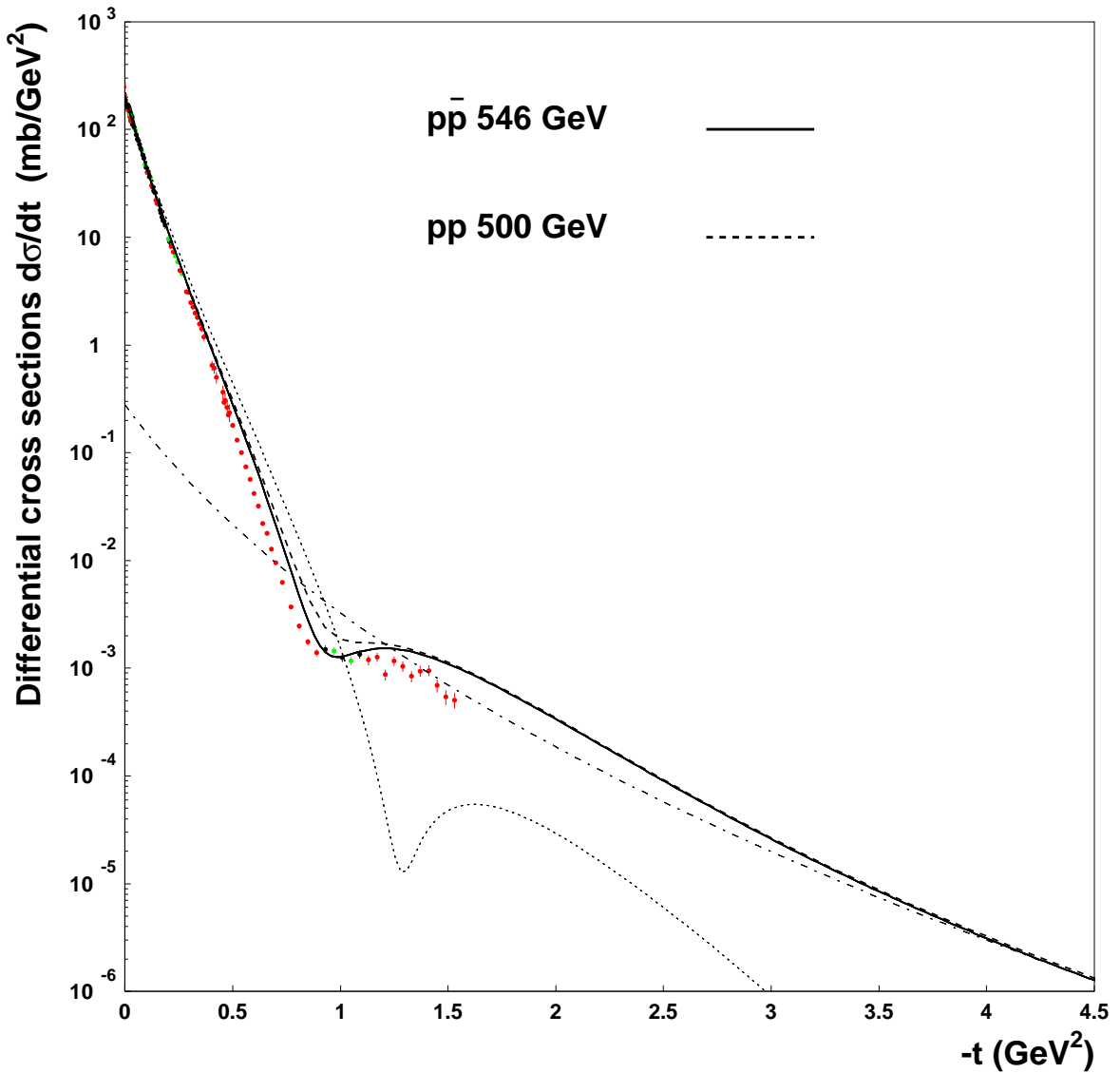


Figure 3: Solid curve represents our calculated  $d\sigma/dt$  for  $\bar{p}p$  at  $\bar{s} = 546$  GeV. Experimental data are from Bozzo et al. [2]. Dotted curve represents  $d\sigma/dt$  due to dihadron alone, while dot-dashed curve represents  $d\sigma/dt$  due to hard-scattering alone. The thick-dashed curve shows our predicted  $d\sigma/dt$  for  $\bar{p}p$  elastic scattering at  $\bar{s} = 500$  GeV, which will be measured at RHIC in the small  $\pmb{t}$  region [15].

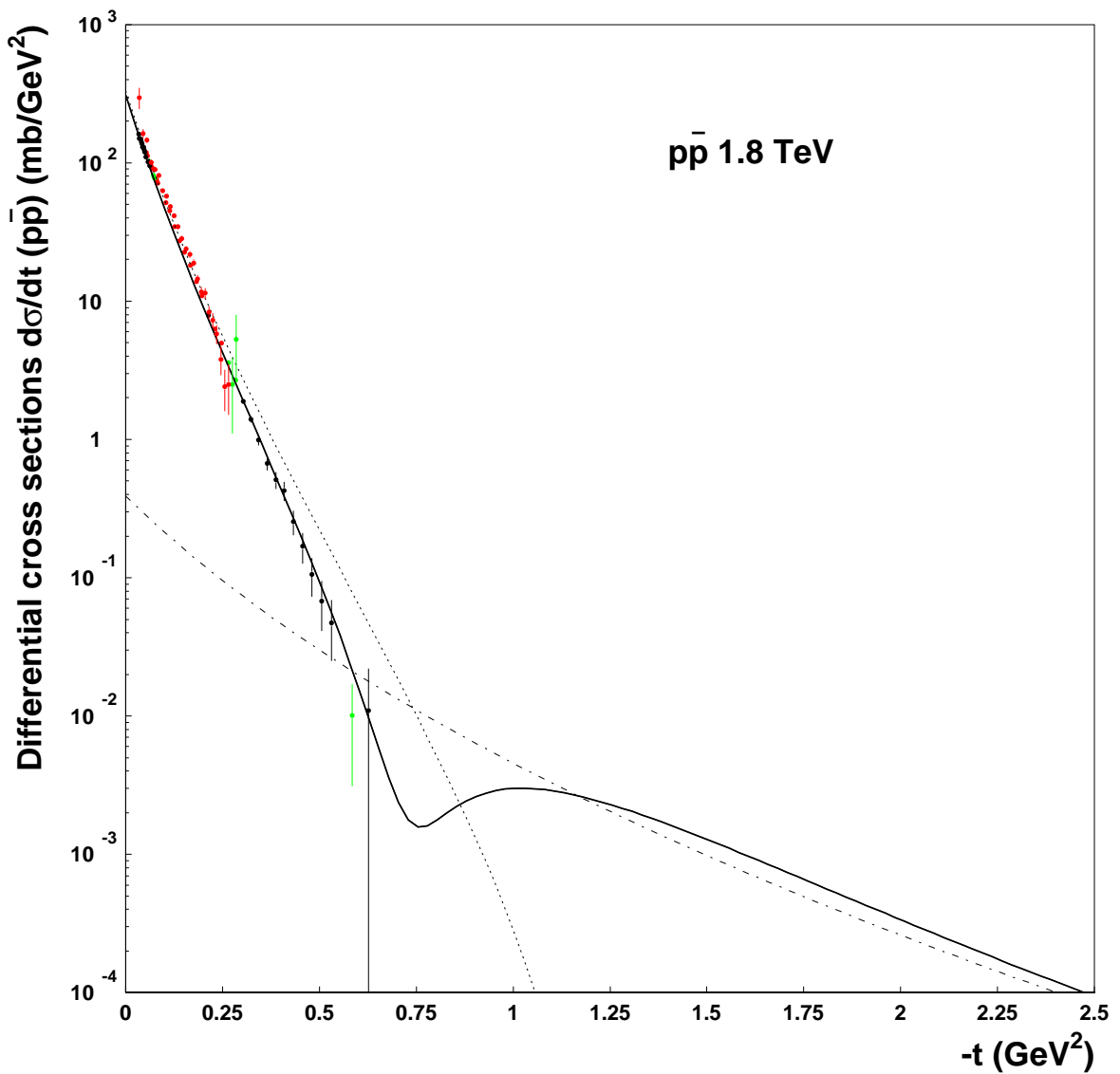


Figure 4: Solid curve represents our predicted  $d\sigma/dt$  for  $p\bar{p}$  at  $\sqrt{s} = 1.8$  TeV with parameters determined from Figs 1, 2, and 3. Experimental data are from Amos et al. [3] and Abe et al. [4]. Dotted curve represents  $d\sigma/dt$  due to diraction alone; dot-dashed curve represents  $d\sigma/dt$  due to hard-scattering alone.

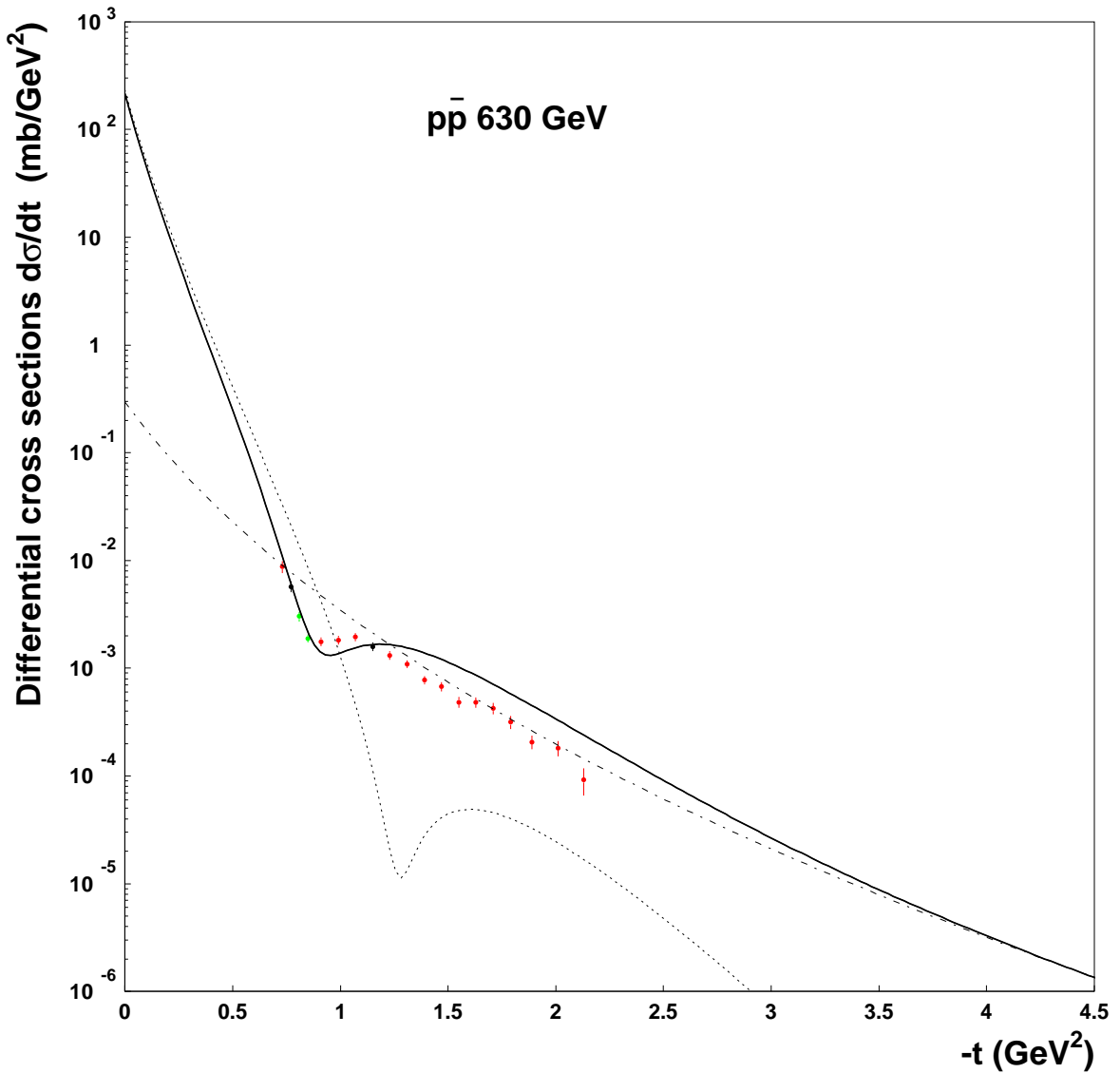


Figure 5: As in Fig.4, solid curve represents our predicted  $d\sigma/dt$  for  $pp\bar{p}$  at  $\sqrt{s} = 630$  GeV with parameters determined from Figs.1,2, and 3. Experimental data are from Bernard et al. [21]. Dotted curve represents  $d\sigma/dt$  due to di-fraction alone; dot-dashed curve represents  $d\sigma/dt$  due to hard-scattering alone.

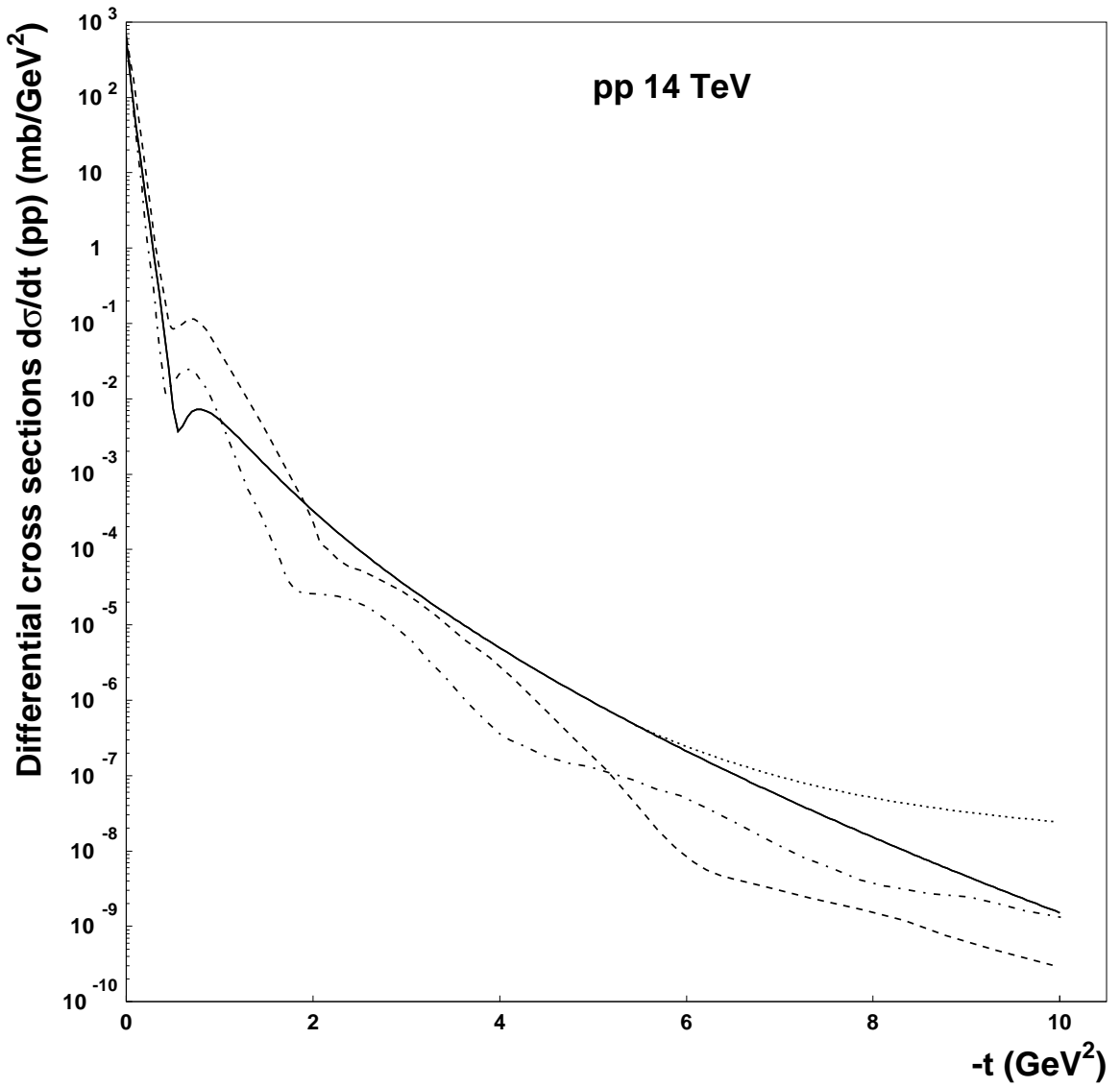


Figure 6: Solid curve shows our predicted pp elastic differential cross section at LHC at the cm energy 14 TeV. Also shown for comparison are  $d\sigma/dt$  predicted by the impact-particle picture model at  $\bar{s} = 14$  TeV (dashed curve) and by the Regge pole-cut model at  $\bar{s} = 16$  TeV (dot-dashed curve) [5], [6], [20]. The dotted line represents schematically a change in the behavior of  $d\sigma/dt$  predicted by our model, because of transition from the nonperturbative regime to the perturbative regime.